Composition of the nuclear periphery from antiproton absorption

P. Lubiński, J. Jastrzębski, and A. Trzcińska
Heavy Ion Laboratory, Warsaw University, PL-02-093 Warsaw, Poland

W. Kurcewicz
Institute of Experimental Physics, Warsaw University, PL-00-681 Warsaw, Poland

F. J. Hartmann, W. Schmid, and T. von Egidy
Physik-Department, Technische Universität München, D-85747 Garching, Germany

R. Smolańczuk and S. Wycech
Sołtan Institute for Nuclear Studies, PL-00-681 Warsaw, Poland
(Received 18 December 1997)

Thirteen targets with mass numbers from 58 to 238 were irradiated with the antiproton beam from the Low Energy Antiproton Ring facility at CERN leading to the formation of antiprotonic atoms of these heavy elements. The antiproton capture at the end of an atomic cascade results in the production of more or less excited residual nuclei. The targets were selected with the criterion that both reaction products with one nucleon less than the proton and neutron number of the target be radioactive. The yield of these radioactive products after stopped-antiproton annihilation was determined using gamma-ray spectroscopy techniques. This yield is related to the proton and neutron density in the target nucleus at a radial distance corresponding to the antiproton annihilation site. The experimental data clearly indicate the existence of a neutron-rich nuclear periphery, a ''neutron halo,'' strongly correlated with the target neutron separation energy B_n and observed for targets with $B_n<10$ MeV. For two-target nuclei ^{106}Cd and ^{144}Sm, with larger neutron binding energies, a proton-rich nuclear periphery was observed. Most of the experimental data are in reasonable agreement with calculations based on current antiproton-nucleus and pion-nucleus interaction potentials and on nuclear densities deduced with the help of the Hartree-Fock-Bogoliubov approach. This approach was, however, unable to account for the ^{106}Cd and ^{144}Sm results. [S0556-2813(98)05206-6]

PACS number(s): 21.10.Gv, 36.10.−k, 25.43.+t

I. INTRODUCTION

There is growing experimental evidence [1–14] that the outer periphery of many stable isotopes of heavy elements is composed predominantly of neutrons. Although this is in agreement with simple [15] as well as sophisticated [16] nuclear models, its recognition could only rarely be found in the literature [17,18]. Indeed, discussions of the differences between matter and charge distributions were generally limited to the comparison of the corresponding mean square radii [19–21], a quantity much more easily accessible to experiment [22,23] than the composition of the nuclear stratosphere (with the nucleon densities two or three orders of magnitude smaller than the central density). Recently, however, interest in the composition of the outermost nuclear periphery was largely increased when it was realized [24–26] that the asymptotic behavior of the nuclear wave function may govern a number of phenomena which are expected in experiments with radioactive beams. In particular, a nonhomogeneous distribution of the extra neutrons (or extra protons) in nuclei far from stability may lead to the existence of a marked neutron (proton) halo. Such halos would certainly manifest themselves, e.g., in low energy transfer reactions induced by radioactive beams or, as recently demonstrated [27], will strongly influence the fusion probability. Before detailed studies of reactions induced by neutron-rich or neutron-poor projectiles are undertaken it is of considerable interest to understand how the nuclear periphery of stable nuclei changes its properties as a function of isospin. If this is well described by existing theories, one can at least hope that an extrapolation to more exotic nuclei and projectiles (with much larger or smaller isospin values than those for stable ones) will be not too far from reality.

This example notwithstanding, the composition and extent of the nuclear periphery are evidently of considerable interest by themselves. Governed by the asymptotic behavior of the nuclear wave function they can be a sensitive testing ground for nuclear models going beyond harmonic oscillator boundaries.

Experimentally, studies of the nuclear periphery are evidently facilitated if the probes used interact very strongly with nucleons leading to clear signals even from the diluted nuclear stratosphere. Indeed, a substantial part of our present information on the extent and composition of the outer nuclear periphery was obtained via the formation of hadronic (pionic, kaonic, and antiprotonic) atoms. Two types of experiments can be performed. In the first one the x-ray spectra of these ''exotic'' atoms are investigated [28–31] and in particular the characteristics of the last x-ray transition which can be observed before the hadron-nucleus interaction prevents further x-ray emission are studied. These characteristics are governed by the hadron-nucleus interaction potential depending in turn on the matter density where the interaction occurred. In the second type of experiments also involving

the formation of hadronic atoms, the characteristics of the hadron annihilation products—mesonic [2,8,9] or nuclear [12]—are studied. The formation and nature of these products depend not only on the nuclear density distribution but are also related to the neutron to proton density ratio.

We have recently reported [12,13] a new experimental study of the nuclear periphery using the formation of antiprotonic atoms. In this study the nuclear products of antiproton annihilation on a peripheral proton or neutron were identified using simple radiochemical methods. It was shown that the outer periphery of the heaviest isotopes of all elements studied is composed to a large extent of neutrons. In addition, a strong correlation between the neutron to proton density ratio and the neutron binding energy was found.

In the present paper we give a more detailed description of this experiment together with some new data.

II. METHOD

After the pure and intense antiproton beam from the LEAR facility at CERN [32–34] became available the yield of the radioactive products formed after a stopped antiproton-target interaction could be investigated. Such studies were undertaken more than ten years ago [35–37] and were continued thereafter [38–40]. Their main objective, similar to that for radiochemical work conducted for decades with protons, heavy ions, or pions (see, e.g., Refs. [41–43]), is the study of the energy transfer to the target nucleus after the interaction. The unusual character of the antimatter projectile, its decay characteristics, and the hope for some exotics add to the interest of such investigations.

Radiochemical experiments with stopped antiprotons were very simple when using the LEAR facility. The extracted extremely pure and monoenergetic antiproton beam was traversing a thin scintillator counter (determining the number of antiprotons) and was impinging on a target thick enough to stop antiprotons. If the antiproton energy was too high, a beam energy degrader was used in front of the target. Preferably the target thickness should be larger than the antiproton path length straggling but this was not always possible with expensive, isotopically separated targets.

An antiproton entering the target material loses energy by the interaction with atomic and conduction electrons. When its kinetic energy is comparable to the ionization energy of the target atoms the antiproton replaces one of the atomic electrons and occupies a high-n orbit of this atom. After the capture an electromagnetic cascade develops through lower, empty (n,l) states. Spatially, as a result of the large antiprotonic mass, a good fraction of this cascade occurs inside the electronic cloud. The energy released by the cascading antiproton is in the beginning of the cascade (when the antiproton is in high-n orbits, close to the electron orbits) taken away by Auger electrons. For lower antiprotonic orbits the emission of electromagnetic radiation becomes important and this x-ray emission dominates for the lowest antiprotonic transitions. The statistical population of the l substates at the moment of capture [44–46] and the selection rules for electromagnetic $E1$ transitions favor the population of highest-l levels $(=n-1)$ at the end of the cascade. Cascading between these circular orbits the antiproton eventually enters the nuclear periphery where, after an encounter with a proton or with a neutron, it annihilates.

As a result, in more than 95% of the annihilations charged and neutral pions are formed with a multiplicity ranging from 2 to 8 and with an average value equal to 5. Some of those pions may enter the nuclear volume, initiating an intranuclear cascade [47–49] and heating the nucleus which subsequently emits neutrons, light charged particles, and intermediate mass fragments or undergoes fission. The development of these processes evidently critically depends on the amount of transferred energy which in turn is related to the number $n_{\rm int}$ of pions directed towards the inner nucleus and interacting inelastically with it. (As a result of the strong pion-nucleus potential, this interaction is generally followed by pion absorption.)

The earliest experimental determination of $\langle n_{\rm int}\rangle$ was presented by Bugg *et al.* [9]. Subsequent experiments are discussed and analyzed by Cugnon *et al.* [50] and the most recent data are due to Polster *et al.* [51]. As could be expected the average value of $n_{\rm int}$ depends on the target mass number A_t and $\langle n_{\rm int}\rangle$ is about 1 for $A_t\approx 200$ and less for lighter target nuclei.

This relatively small value of the average number of pions interacting with the target nucleus immediately indicates that annihilation events with $n_{\rm int}=0$ should occur with substantial probability. This is, indeed, confirmed by intranuclear-cascade calculations [52] which predict that these ''void cascade events'' appear in 10–20 % of the annihilations. After such events cold residual nuclei are formed with a mass equal to the target mass decreased by the mass of one nucleon which participated in the annihilation process. Experimentally, such products with mass (A_t-1) were clearly observed with a large yield in radiochemical studies of the stopped-antiproton interaction with nuclei [36,38].

In the Nuclear Chart one can find a number of target nuclides for which both neighboring products with one nucleon less than those in the target with mass number $A_t=N_t+Z_t$ are radioactive. For such target nuclei the yield ratio of the (N_t-1) to the (Z_t-1) products after annihilation, easily determined using classical nuclear spectroscopy methods, will give information on the neutron to proton ''concentration ratio'' in the region where annihilation occurred.

Information on the annihilation site can also be obtained from such a simple radiochemical experiment providing the fraction $Y(A_t-1)$ of annihilation events leading to the (A_t-1) products is determined. This fraction depends on the product of the antiproton annihilation probability $W(r)$, where r is the radial distance from the center of the nucleus, with $P_{\rm miss}(r)$. The last quantity expresses the ''missing probability'' [12] that all pions created during the antiproton annihilation miss the inner nucleus, leading to $n_{\rm int}=0$. $P_{\rm miss}(r)$ evidently increases with the radial distance r. Therefore qualitatively, the larger the $Y(A_t-1)$ value is, the farther from the nuclear center the neutron to proton ratio is tested.

The experiment determines the yield ratio of (N_t-1) to (Z_t-1) products and the fraction of events leading to (A_t-1) nuclei. To interpret the data and to know at which radial distance the method tests the composition of the nuclear periphery, recourse to the theory is necessary. Recent calculations indicate [53] that almost independently of the target mass the antiproton annihilation probability $W(r)$ has its

TABLE I. Characteristics of the antiproton beam.

Experiment	Beam momentum [MeV/c]	Beam energy [MeV]	Measured path length straggling Target	FWHM [mg/cm^2]	Calculated path length straggling[a] FWHM [mg/cm^2]
1991	205.5	22.5	^{232}Th	64±4	57.4
			^{197}Au	56±3	57.4
1992	200.4	21.4	^{27}Al	22.5±1.0	21.9
1993	200.4	21.4	^{27}Al	21.9±1.0	21.9
1995	310.1	49.9			
1996	106.0	6.0	^{27}Al	4.6±0.4	2.9

[a]Reference [71].

maximum value at distances about 2 fm larger than the half-density radius. Its convolution with $P_{\rm miss}(r)$ locates the maximum of $n_{\rm int}=0$ events at a distance even about 1 fm larger, making the method sensitive to the composition of the outermost nuclear periphery with nuclear densities of about 10^{-2}–10^{-3} of the central density. We shall come back to these questions at the end of this paper.

In order to be able to compare the experimental data for any measured target, independently of its neutron to proton ratio, we introduce the neutron halo factor defined as

$$f_{\rm halo}^{\rm periph}=\frac{N(\bar{p},n)}{N(\bar{p},p)}\,\frac{{\rm Im}(a_p)}{{\rm Im}(a_n)}\,\frac{Z_t}{N_t},$$

where $N(\bar{p},n)/N(\bar{p},p)$ is the ratio of produced A_t-1 nuclei, and a_n and a_p are the $\bar{p}$-n and $\bar{p}$-p scattering amplitudes, respectively [10]. The ratio ${\rm Im}(a_p)/{\rm Im}(a_n)=1/R_{np}$ accounts for the ratio of annihilation probabilities. A similar halo factor was previously introduced by Bugg *et al.* [9] who investigated the composition of the nuclear periphery determining the characteristics of mesonic products of antiproton annihilation. In their method all annihilation events contributed to the halo factor, whereas only the most peripheral events are of importance in the present method; so the superscript ''periph'' is used here.

Neglecting the corrections mentioned below, the halo factor accounts essentially for the enhancement of the neutron or proton concentration over the normal one (i.e., that which reflects the N/Z target ratio) in the tested nuclear region. A halo factor higher than 1 would indicate an increased neutron concentration (''neutron halo'') whereas $f_{\rm halo}^{\rm periph}<1$ would correspond to an enhanced proton density at the nuclear periphery.

There are, however, corrections which have to be discussed. The above considerations assume that all events in which $n_{\rm int}=0$ lead to cold nuclei with mass number (A_t-1). This is not necessarily the case. Microscopically, the nuclear periphery may contain some amplitudes of states bound more strongly than the nucleon separation energies or fission barrier of these (A_t-1) nuclei. In such a case antiproton annihilation on these deeply bound states would lead to high rearrangement energies [54] of the (A_t-1) products, which would subsequently emit particles or fission. A simple Thomas-Fermi model estimate [55] of this effect or more detailed calculations within the Hartree-Fock-Bogoliubov model reported in Ref. [53] show that this can affect the halo factor by no more than 30%.

Another effect which merits consideration is the possibility of the pion charge exchange process which could change the final population of (Z_t-1,N_t) and (Z_t,N_t-1) nuclei. The yield of this process was determined experimentally and is discussed in Sec. IV C.

Ending this section about the experimental method one should mention the article by Bloom *et al.* [56], known to us well after the first presentation [12,13] of the method described here. In this article the idea of looking on nuclear (rather than mesonic) signals when investigating the composition of the nuclear periphery with exotic atoms was already suggested. To the best of our knowledge these suggestions were never realized in the way proposed there.

III. EXPERIMENTAL TECHNIQUE

The experimental results which are presented in this paper were gathered during five irradiation series from 1991 to 1996. The antiproton beam momenta delivered by the LEAR facility are listed in Table I.

A similar setup was employed for the experiments with 200 and 310 MeV/c antiprotons. After passing through a 18.5 mg/cm^2 beryllium window at the end of the beam tube and after traversing approximately 10 cm of air, the antiprotons encountered the first scintillation counter S1 ($\phi=15$ mm, thickness 10 mm) with a central hole of 7 mm. This counter, used also for beam focusing, served as an active diaphragm for antiproton counting during the target irradiation.

A variable-thickness plastic beam energy degrader was placed immediately after the S1 counter. Its selected thickness was calculated to ensure that the antiproton beam, after traversing the second scintillation counter S2 ($\phi-7$ mm, thickness 2.5 mm) and a few Al foils (with a total thickness of about 80 mg/cm^2), stopped approximately in the middle of the irradiated target. Similar Al foils were also placed behind the target. The ^{24}Na activity produced by antiprotons stopped in the backward and forward Al foils was used to determine the fraction of the antiprotons which triggered the S2 counter but were not stopped inside the target material. This was due to the fact that the target thickness (indicated in Table II) was generally smaller than the antiproton path length straggling (shown in Table I and in Fig. 1) induced

TABLE II. Targets and numbers of stopped antiprotons.

Target	Enrichment [%]	Physical form	Thickness [mg/cm^2]	$\bar{p}$ stopped in target [10^8]	Experiment
^{45}Sc	99.9	metal	55.8	3.4±0.2	1992
^{56}Fe	99.9	metal	43.6	9.4±0.9	1993
^{58}Ni	99.9	metal	40.1	7.4±0.3	1992
^{58}Ni	99.8	metal	60.1	2.9±0.2	1996
^{96}Zr	85.3	metal	35.2	2.2±0.3	1992
^{96}Zr	85.3	metal	35.2	5.6±0.3	1996
^{96}Ru	97.9	powder+glue	20.1	0.7±0.2	1992
^{96}Ru	97.9	powder+glue	20.1	0.7±0.2	1996
^{nat}Cd	^{106}Cd (1.26%)	metal	37.5	1.8±0.2	1993
^{nat}Cd	^{106}Cd (1.26%)	metal	39.0	7.1±0.3	1996
^{106}Cd	76.5	metal	40.0	2.1±0.3	1993
^{106}Cd	76.5	metal	40.0	7.6±0.4	1996
^{128}Te	98.3	metal	353	9.1±1.0	1995
^{128}Te	98.3	metal	91.1	3.2±0.2	1996
^{nat}Te	^{130}Te (33.9%)	powder+glue	104	0.9±0.2	1992
^{130}Te	99.6	powder+glue	37.8	9.3±2.0	1993
^{130}Te	99.3	powder+glue	93.6	2.3±0.2	1996
^{144}Sm	96.5	metal	47.2	3.1±0.2	1992
^{144}Sm	86.6	metal	45.7	14±3	1993
^{144}Sm	90.8	metal	109	6.1±0.3	1996
^{148}Nd	91.6	powder, oxide	95	1.8±0.4	1993
^{148}Nd	88.6	powder, oxide	90	4.1±0.4	1996
^{nat}Eu	-	powder+glue, oxide	105	3.2±0.4	1992
^{154}Sm	97.7	metal	54.4	3.2±0.5	1992
^{154}Sm	98.3	metal	107	1.3±0.1	1996
^{160}Gd	98.1	powder+glue, oxide	40.7	9.8±2.0	1993
^{160}Gd	98.1	powder+glue, oxide	110	4.4±0.4	1996
^{nat}Yb	^{176}Yb (12.7%)	metal	102	0.8±0.1	1992
^{176}Yb	96.4	metal	31.1	9.8±2.0	1993
^{176}Yb	96.4	metal	114	8.6±0.5	1996
^{206}Pb	95.9	metal	85.7	15±2	1993
^{232}Th	100	metal	100	23±1	1991
^{232}Th	100	metal	4.54	0.9±0.3	1993
^{232}Th	100	metal	43.0	1.5±0.3	1993
^{238}U	99.8	metal	107	5.2±0.2	1992

during the energy degradation by the moderator, S2 counter, and target material. The yield for producing ^{24}Na in the stopped-antiproton interaction with Al target was determined by independent measurements. The average value found was 19.5±1.0 ^{24}Na nuclei produced per 1000 $\bar{p}$. The path length straggling shown in Table I was determined by activation analysis, measuring the activity induced by stopped antiprotons in the target composed of a stack of thin foils.

Depending on the half-life of the (A_t-1) reaction products, each target stack was bombarded by a short (10–15 min) or long (80–90 min) antiproton ''spill,'' totaling about 5×10^8–10^9 particles. Generally more than a half of these antiprotons were stopped by the target material, whereas the rest reacted with Al or other target components (glue, oxygen). In Table II the targets used in the present work are listed together with the integrated intensities of antiprotons stopped in the target nuclei.

Slight modifications of the above-described irradiation

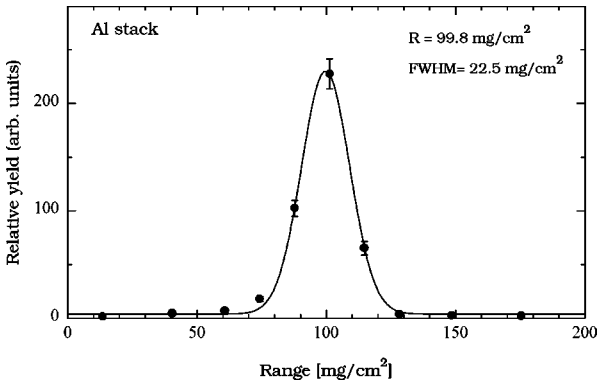

FIG. 1. Example of the measured antiproton range distribution in an Al stack, determined by counting the produced ^{24}Na activity. Before impinging on the Al stack the antiproton energy, equal to 21 MeV, was degraded in 800 μm of Mylar and in 2.5 mm of a plastic scintillator.

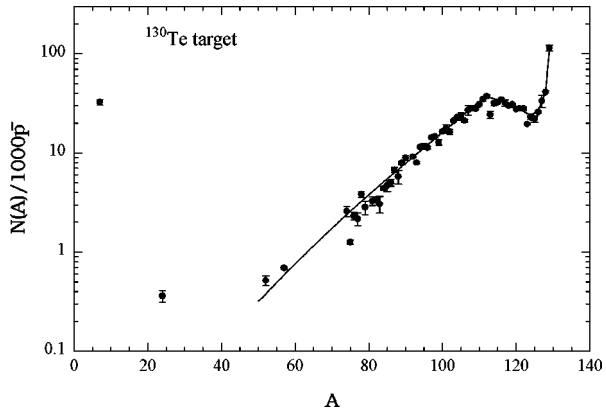

FIG. 2. Mass yield distribution for the ^{130}Te target. The method for the determination of this distribution is given elsewhere [40,58].

conditions were introduced for the last run, where the antiprotons with the lowest momentum were available. During this run the S1 counter with a $\phi=8$ mm central hole and 1 mm thickness preceded the S2 counter with a 100 μm scintillator. Both these counters were placed in a light-tight chamber filled with He gas to decrease both the slowing down and scattering of the low-energy beam. Al windows of 12 μm thickness were put at the entrance and exit of the He chamber. Eventually, the 6.0 MeV energy delivered by the LEAR facility was degraded to 2.8 MeV, with only a rather small energy straggling, as indicated in Table I. This beam was impinging on the target material, with this time large Al foils placed only behind the target to control the beam scattering off the targets (diameter 10 mm).

Shortly after the end of the irradiation (about 2 min in the case of short-lived (A_t-1) products) the gamma-ray counting was started using HPGe coaxial detectors of about 10–30 % relative efficiency and with an energy resolution slightly below 2 keV for the ^{60}Co 1333 keV transition. In some cases, when the low-energy gamma rays were of interest, a planar HPGe detector with an energy resolution of about 600 eV at 122 keV energy was also employed. The gamma-ray counting was generally continued for a few days at CERN and later, for many months in Warsaw, where in addition a 60% HPGe detector was used. The production yield of (A_t-1) nuclei was deduced from the absolute intensities of their characteristic gamma lines (followed for a few half-lives) after corrections for the decay during and after the irradiation. To this end the antiproton beam intensity as a function of time was always carefully monitored. Generally half-lives, energies, and branching ratios were taken from the most recent Nuclear Data compilations, available via an internet connection. In some cases also Ref. [57] was used.

For some targets the total number of antiprotons stopped in the target material was additionally determined by integrating the mass yield distribution of heavy reaction residues. These distributions were gathered from the yield of the radioactive reaction products, as previously described [38,39]. It was assumed that for nonfissile targets one antiproton stopped in the target material produces one heavy reaction residue. The total number of antiprotons determined in this way was in general within 10–15 % equal to the number obtained using the indications of S2 counter with the corrections described above. Figure 2 shows as an example the mass yield distribution obtained for the ^{130}Te target. More information on experimental details and evaluation procedures pertaining to each particular target is presented in Refs. [58,59].

IV. EXPERIMENTAL RESULTS

A. Peripheral neutron to proton density ratio

The final results, used to determine the peripheral neutron to proton density ratios, are presented in Table III. These data supersede those previously published by Lubiński *et al.* [13]. The differences are in some cases due to more recent information on the decay properties of the (A_t-1) nuclei and, in other cases, to the inclusion of results gathered during the 1995 and 1996 runs. The second, third, and fourth columns of this table give the absolute production yield of nu-

TABLE III. Absolute production yield of A_t-1 nuclei, their yield ratio, and peripheral halo factor.

	Produced nuclei				
Target	$\frac{N_t-1}{1000\bar{p}}$	$\frac{Z_t-1}{1000\bar{p}}$	$\frac{A_t-1}{1000\bar{p}}$	$\frac{N(\bar{p}n)}{N(\bar{p}p)}$	$f_{\text{halo}}^{\text{periph}}$
$^{58}_{28}$Ni	45±4	49±7	94±6	0.90±0.12	1.3±0.2
$^{96}_{40}$Zr	111±18	34±8	145±11	3.3±0.6	3.7±0.6
$^{96}_{44}$Ru	39±10	50±14	89±16	0.79±0.17	1.1±0.2
$^{106}_{48}$Cd	33±6	72±11	105±8	0.5±0.1	0.6±0.1
$^{128}_{52}$Te	65±17	17±3	82±14	3.9±1.0	4.3±1.1
$^{130}_{52}$Te	81±16	20±4	101±12	4.0±0.4	4.2±0.4
$^{144}_{62}$Sm	⩽31	94±20	110±8	⩽0.4	⩽0.5
$^{148}_{60}$Nd	56±7	13±4	69±8	4.4±0.9	4.8±0.9
$^{154}_{62}$Sm	77±11	39±8	116±10	2.0±0.3	2.2±0.4
$^{160}_{64}$Gd	94±23	17±5	111±25	5.5±1.8	5.8±1.9
$^{176}_{70}$Yb	196±28	26±6	222±25	7.6±0.6	8.0±0.6
$^{232}_{90}$Th	71±12	13±2	84±11	5.4±0.8	5.4±0.8
$^{238}_{92}$U	91±7	19±2	110±7	5.8±0.8	5.8±0.8

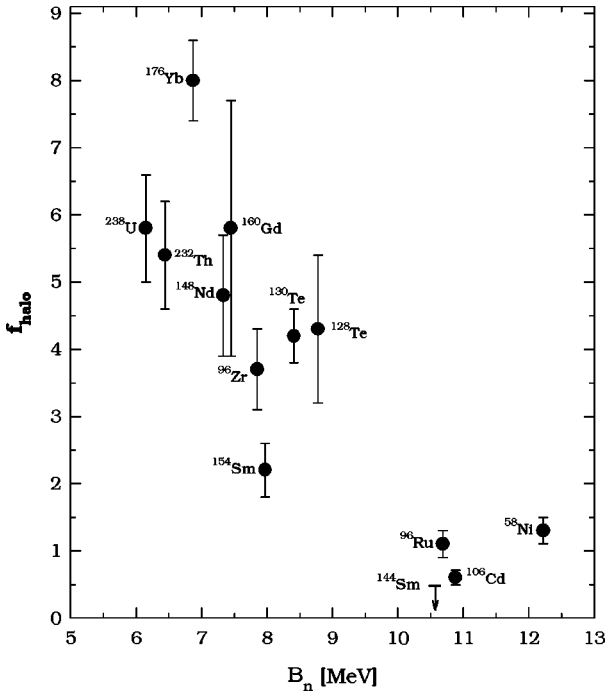

FIG. 3. Neutron halo factor (defined in the text) as a function of the target neutron separation energy B_n.

clei one mass unit lighter than the target mass. The halo factor $f_{\rm halo}^{\rm periph}$, presented in the last column of this table, was obtained from the measured ratio of the produced (N_t-1) nuclei to the (Z_t-1) ones (column 5) after correction for the target Z_t/N_t ratio and for the ratio of the antiproton annihilation probabilities on a neutron to that on a proton, R_{np}. Following Bugg *et al.* [9] the value of the last ratio was taken to be equal to 0.63, in agreement with Ref. [60]. Its error is not included in the errors of $f_{\rm halo}^{\rm periph}$ in Table III.

The data from Table III are also shown in Figs. 3–5. Figure 3 presents the halo factor as a function of the target neutron separation energy. The negative correlation, previously observed [13] for a smaller data sample, is confirmed. The unusually large error for the ^{160}Gd target is due to the poorly known absolute transition intensities in the decay of (A_t-1) products [61] of this target. The largest value of the halo factor is obtained for the ^{176}Yb target and is discussed

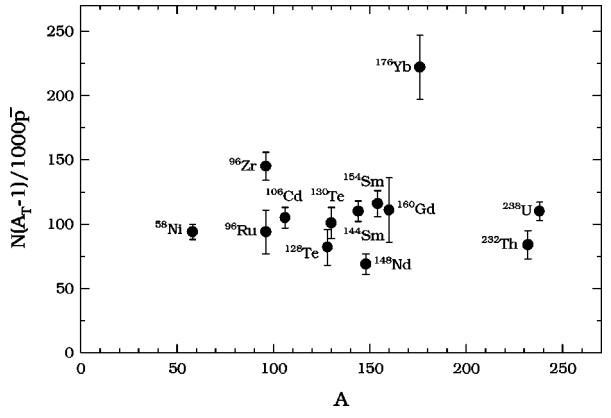

FIG. 4. Absolute production yield of isotopes A_t-1 having one mass unit less than the target mass as a function of the target mass number.

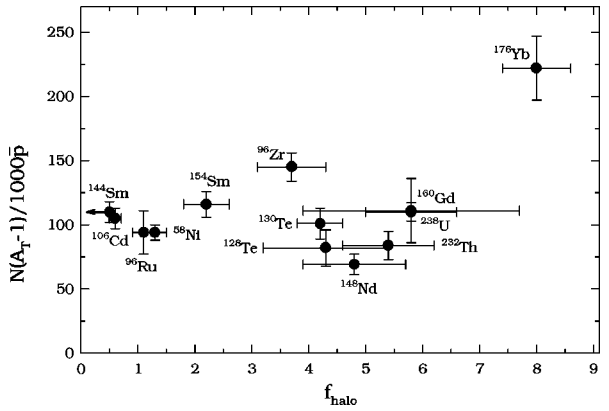

FIG. 5. Correlation between halo factor and absolute production yield for A_t-1 nuclei.

below. For two investigated nuclei ^{106}Cd and ^{144}Sm, the measured halo factor is substantially smaller than 1. As our assumed value of the ratio $\mathrm{Im}(a_n)/\mathrm{Im}(a_p)$ is probably the lowest acceptable (see the discussion in [53]), these results clearly indicate the proton-rich atmosphere of these two nuclei. (This would remain true for ^{144}Sm even if one assumes a value $R_{np}=0.48$ as obtained in the ^{4}He experiment [62].) The systematics presented in Fig. 3 show that nuclei with a smaller neutron binding energy exhibit, on the contrary, a periphery rich in neutrons—a ''neutron halo'' in the terminology introduced more than a quarter of a century ago [2,5,9].

Figure 4 shows, as a function of the target mass, another observable of the present experiment, namely, the absolute yield (per 1000 antiprotons) of the production of nuclei with one nucleon less than the target mass. For all but the ^{176}Yb target this yield is close to 10%, without any noticeable dependence on the target mass number. The correlation of two observables, the halo factor, and the yield of (A_t-1) nuclei, presented in Fig. 5, demonstrates again the unusual character of the results obtained for ^{176}Yb.

B. Isomeric ratios

If one of the (A_t-1) products has an isomeric state with low excitation energy, the peripheral antiproton annihilation can populate, besides the ground state, also this isomer. Table IV shows the experimentally determined isomeric ra-

TABLE IV. Isomeric ratios for A_t-1 nuclei.

Isomer	Spin	Energy [keV]	Isomeric ratio
^{44}Sc$(m)/^{44}$Sc(g)	$6^+/2^+$	271/0	0.42 ± 0.05
^{95}Tc$(g)/^{95}$Tc(m)	$\frac{9}{2}^+/\frac{1}{2}^-$	0/39	0.58 ± 0.22
^{127}Te$(m)/^{127}$Te(g)	$\frac{11}{2}^-/\frac{3}{2}^+$	88/0	$\leqslant 0.6$
^{129}Te$(m)/^{129}$Te(g)	$\frac{11}{2}^-/\frac{3}{2}^+$	105/0	0.45 ± 0.15
^{129}Sb$(m)/^{129}$Sb(g)	$\frac{19}{2}^-/\frac{7}{2}^+$	1851/0	$\leqslant 0.02$
^{150}Eu$(m)/^{150}$Eu(g)	$5^{(-)}/0^{(-)}$	42/0	$\leqslant 1.3$
^{152}Eu$(2)/^{152}$Eu(g)	$(8)^-/3^-$	148/0	$\leqslant 0.016$
^{152}Eu$(g)/^{152}$Eu(1)	$3^-/0^-$	0/46	$\leqslant 5.7$
^{152}Eu$(2)/^{152}$Eu(1)	$(8)^-/0^-$	148/46	0.11 ± 0.03
^{196}Au$(m)/^{196}$Au(g)	$12^-/2^-$	595/0	$\leqslant 0.02$

tios. Not considering the $3^-/0^-$ isomeric pair in ^{152}Eu (where the experimental limit is too high to be significant) the high-spin/low-spin formation ratio is always smaller or substantially smaller than 1.

This is in marked contrast to the isomeric ratios determined for the deep spallation products after stopped-antiproton annihilation on nuclei [36,38]. In this case, as a result of the emission of energetic particles in the cascade process, the final nuclei acquire a considerable angular momentum, which is reflected by a preferential production of high-spin isomers. In the case of (A_t-1) nuclei the isomeric ratio depends on the microscopic composition of the nuclear periphery around the annihilation site. The contribution of the high-spin components is lowered there due to the centrifugal barrier but may be increased due to a larger occupation number in comparison with the low-spin components. Evidently, in the discussion of the isomeric ratio for (A_t-1) nuclei the feeding of isomers by shorter-lived states with excitation energies below the particle emission threshold should be also considered. Although such a discussion for all measured cases would be outside the scope of this experimental paper, we present below in some detail one particularly simple example (^{129m,g}Te). We hope that other cases given in Table IV may be sometimes used to furnish a supplementary check for the calculations of the nuclear periphery.

C. Charge exchange reactions

The charge exchange process was claimed [63] as mainly responsible for the larger number of π^- events in heavy than in light nuclei in antiproton annihilation data reported by Bugg *et al.* [9]. (Bugg *et al.* attributed this difference to the neutron halo effect in heavy nuclei.) In the present method the simulation of a neutron halo or at least the increase of the observed effect could be due to the transformation of the (N_t, Z_t-1) annihilation products to (N_t-1, Z_t) ones via $\pi^0\rightarrow\pi^-$ or $\pi^+\rightarrow\pi^0$ charge exchange reactions occurring between annihilation pions and the inner nucleus (if they could proceed without a substantial excitation of this nucleus). Although such a transformation is evidently undetectable by our experimental method, we can estimate its importance by looking for the formation of (Z_t+1) nuclei, possible only via the same charge exchange processes.

The determined upper limits for the production of (Z_t+1) nuclei are presented in Table V. The comparison of the absolute yields of these nuclei with yields presented in the second and third column of Table III clearly indicates that the charge exchange effects are generally much smaller than the experimental errors assigned to the production yields of nuclei determining the halo factor. Therefore, in agreement with arguments presented in Ref. [11], we will in the present work ignore the corrections which could result from these processes. This is not in contradiction with the results of Refs. [36,37], where two (Z_t+1) products were observed. Their absolute yields were, however, not much larger than the upper limit values presented in Table V.

TABLE V. Upper limits for the production of Z_t+1 isotopes by pion charge exchange.

Target	Isotope	Spin	$\frac{N(Z_t+1)}{1000\overline{p}}$	$\frac{N(A,Z_t+1)}{N(A_t,Z_t)}$
^{56}Fe	^{55}Co	$7/2^-$	$\leqslant 0.24$	$\leqslant 0.006$[a]
^{96}Zr	^{95}Nb(m)	$1/2^-$	$\leqslant 1.3$	$\leqslant 0.038$
	^{95}Nb(g)	$9/2^+$	$\leqslant 0.5$	$\leqslant 0.015$
^{96}Ru	^{95}Rh(m)	$1/2^-$	$\leqslant 6.2$	$\leqslant 0.12$
	^{95}Rh(g)	$5/2^+$	$\leqslant 5.5$	$\leqslant 0.11$
^{206}Pb	^{205}Bi	$9/2^-$	$\leqslant 0.7$	$\leqslant 0.009$[b]
	^{204}Bi	6^+	$\leqslant 0.7$	$\leqslant 0.009$[b]
	^{203}Bi	$9/2^-$	$\leqslant 1.8$	$\leqslant 0.023$[b]

[a]Production of Z_t nuclei assumed to be equal to 40 per 1000 antiprotons, from systematics based on the $N(Z_t)$ dependence on the neutron binding energy B_n.

[b]Production of Z_t nuclei assumed to be equal to 80 per 1000 antiprotons.

V. DISCUSSION

The method presented in this work has allowed us to correlate in a quantitative way neutron enhancement in the nuclear periphery with the neutron separation energy values B_n. The data presented in Fig. 3 indicate that isotopes having B_n smaller than about 10 MeV exhibit a nuclear periphery in which the neutron density is larger than that expected from the N/Z ratio of a given nucleus. As the neutron separation energy for the heaviest isotopes of all naturally occurring elements is generally below 10 MeV, the enhancement of the nuclear periphery with neutrons should be a quite common phenomenon. In the following section we will show that this observation is in qualitative agreement with expectations based on the Hartree-Fock-Bogoliubov approach, a model commonly used [16] to describe the properties of the nuclear periphery. To compare the experimental results with theory in a more quantitative way the antiproton-nucleus interaction should be considered. This was thoroughly discussed in a previous paper by some of us [53] and is also briefly outlined below.

A. Nuclear periphery from HFB calculations

In the present paper we concentrate on the description of the nuclear periphery using a self-consistent Hartree-Fock-Bogoliubov (HFB) model. We are perfectly aware of the limitations inherent to this model. One of them, namely, the unability to correctly predict the binding energies, is probably the most troublesome for an approach in which the binding energy is used to correlate one of the experimental observables. This was the reason why in our previous papers [13,53] we also investigated another very simple asymptotic density model [15] in which a number of phenomenological inputs, including binding energies, was used. However, the agreement with the experiment was apparently not improved in comparison with the HFB model. Therefore, at the present stage of this research we concentrate on the HFB method. We hope that in future works our experimental data will allow one to discriminate between different approaches [64] modeling the nuclear periphery.

We have applied a HFB code which uses the coordinate representation and solves the HFB equation on a spatial mesh. For the Skyrme interaction, the HFB equation is a

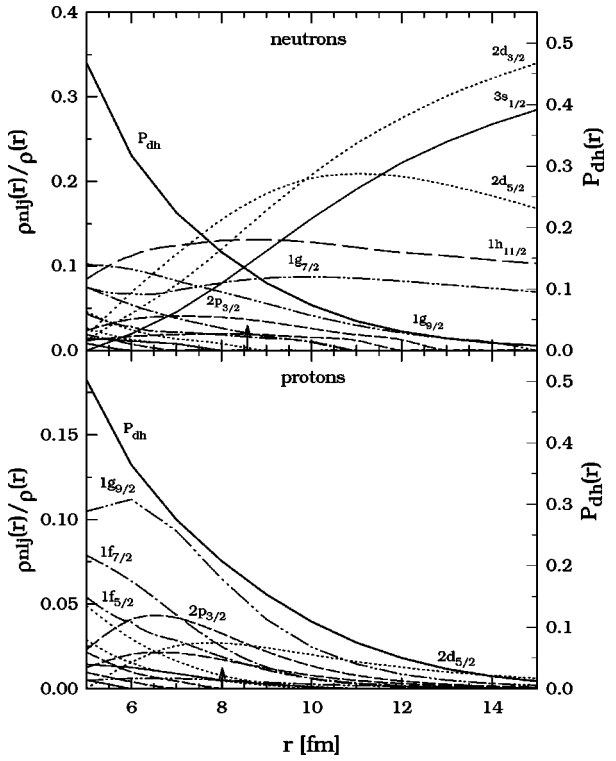

FIG. 6. Relative contribution of the individual shell model orbitals to the total neutron and proton densities in ^{130}Te as a function of the radial distance, obtained using the Hartree-Fock-Bogoliubov approach. The curve marked P_{dh} shows the contribution of orbitals bound by more than the neutron separation energy. The arrows indicate the most probable distance of annihilation on a neutron (upper part) and on a proton (lower part), respectively.

differential equation in spatial coordinates. In our calculations, we used the SKP version of the Skyrme interaction [65]. As a result of the imposed spherical symmetry, the HFB+SKP model is solved separately for each partial wave (j,l). We used 100 mesh points in the radial coordinate in a box of size 25 fm. As a boundary condition, we demanded the wave functions to vanish at the far end of the box.

The above-described method gives the amplitude of the wave functions which can be followed to large distances from the nuclear center. The contribution of each orbital to the nuclear density is given by the square of this wave function at a given radius times the occupation number for this orbital. Particle wave functions are normalized in such a way that the trace of the Hermitian density matrix for protons (neutrons) is equal to the proton (neutron) number. For large radial distances the centrifugal barrier suppresses the contribution of high-j orbitals in comparison with those with small j. (This effect is illustrated in Figs. 3 and 4 of Ref. [17].) The centrifugal barrier effect may be compensated for or overcome by the occupation number for high-j orbitals. As a result, both low- and high-spin orbitals contribute to the composition of the nuclear periphery. Figure 6 gives an example of the calculated composition of the nuclear periphery for the ^{130}Te isotope. The antiproton annihilation leads to a hole in one of the indicated orbitals. The corresponding hole-excitation state will decay by gamma or conversion electron emission to the ^{129}Te or ^{129}Sb ground state. In the case of ^{129}Te annihilation can also lead to the excitation of the $h11/2$ isomer. (The 19/2 isomer in ^{129}Sb has a three-quasiparticle nature [66] and, evidently, cannot be excited directly by antiproton annihilation on any ^{130}Te proton orbital. This is in agreement with the experimental result given in Table IV.)

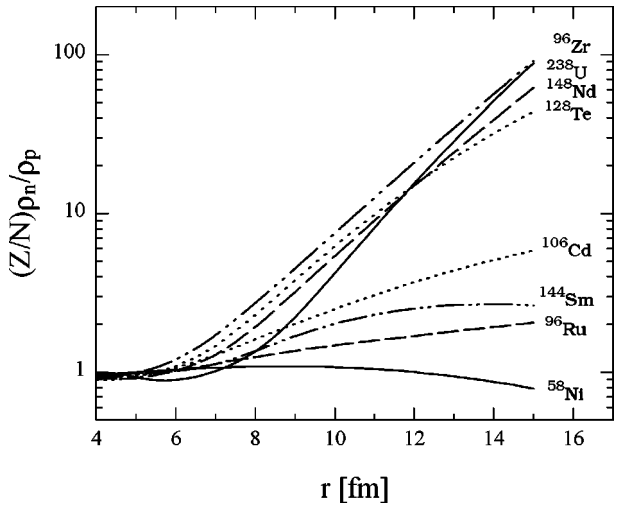

FIG. 7. Calculated (HFB method) neutron to proton density ratio as a function of the nuclear distance for some investigated isotopes.

Figure 6 shows the amplitudes of orbitals contributing to the composition of the nuclear periphery. Among these states some are so deeply bound that the antiproton annihilation on them leads to excitation energies of (A_t-1) nuclei larger than the neutron separation energy (or proton separation energy + Coulomb barrier or fission barrier). These ''deep hole'' states will evidently decay by particle emission, affecting the primary population of the (A_t-1) nuclei. The total contribution of these states to the composition of the nuclear periphery is also indicated in Fig. 6. Around the antiproton annihilation site (discussed in more detail below) this contribution does not exceed 30% for all cases discussed in this work.

Figure 7 presents the calculated ratio of the (normalized) neutron to proton densities as a function of the radial distance for some target isotopes indicated in Table III. The experimentally observed neutron-rich periphery for isotopes with a neutron separation energy smaller than 10 MeV is qualitatively confirmed by the calculated densities. On the contrary, the proton-rich nuclear atmosphere observed for ^{106}Cd and ^{144}Sm ($f_{\rm halo}^{\rm periph}<1$) is not expected by the theory.

Figure 8 shows the absolute values of the calculated neutron and proton density for the ^{96}Zr isotope. Figure 9, finally, displays the neutron to proton density ratio as a function of the radial distance for a series of even Zr isotopes. The gradual ''buildup'' of the neutron atmosphere with increasing mass number is clearly shown by this calculation. The figure presents, besides stable isotopes, the theoretical expectation for isotopes up to 8 mass units heavier or lighter than the stable ones. It illustrates what may be expected when experiments with moderately changed isospin become feasible.

B. Antiproton-nucleus interaction

The interactions in question involve three distinctly separate stages. (1) The initial atomic state of the antiproton is

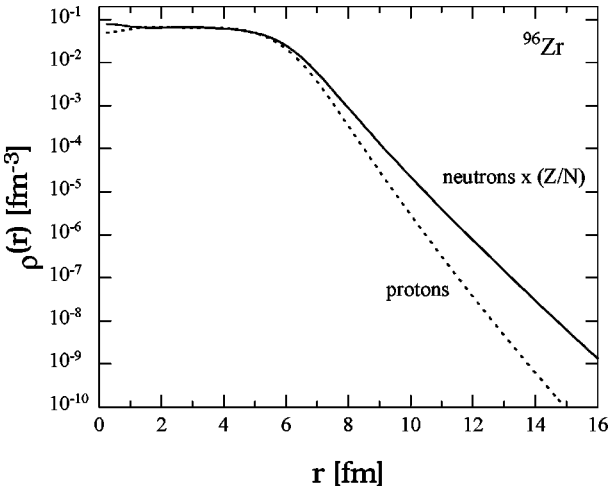

FIG. 8. Calculated neutron and proton densities for ^{96}Zr.

determined by the long-range Coulomb interaction. At nuclear distances, however, the atomic wave function $\Phi_{\bar{N}}$ is determined by the centrifugal barrier and an antiproton-nucleus optical potential. (2) The next stage consists of antiproton annihilation on a nucleon leading to final mesons. This process lies beyond the present theoretical description and must be discussed in a phenomenological way in terms of the pion multiplicity and energy distribution. (3) The final pions undergo elastic and inelastic nuclear reactions. The radiochemical method filters these to the elastic channel.

Each stage is fairly complicated and requires an approximate description. Fortunately there are two simplifying effects: the strong absorption of the antiproton and pions and the large energy release in the annihilation act. It is this energy release that allows us to use the closure approximation over the final nuclear states. As a consequence one can obtain [53] a semiclassical formula for the partial absorption width on a single nucleon i,

$$\Gamma = 4\frac{\pi}{\mu_{N\bar{N}}}\mathrm{Im}a_{N\bar{N}}\int |\Phi_{\bar{N}}(\mathbf{Y})|^2 \nu(\mathbf{Y}-\mathbf{X})\rho_i(\mathbf{X}) \times[1-P_{dh}(\mathbf{X})]P_{\mathrm{miss}}\left(\frac{\mathbf{X}+\mathbf{Y}}{2}\right)d\mathbf{Y}d\mathbf{X}. \quad (1)$$

Here $\mathbf{Y}$ is the antiproton coordinate and $\mathbf{X}$ is the nucleon coordinates. The $\mu_{N\bar{N}}$ is the reduced mass of $N\bar{N}$ system and ρ_i is the nuclear density for protons or neutrons, given by a sum over single nucleon states, $\rho=\Sigma_a\phi_a^2$. This density is folded over a form factor $\nu(Y-X)$ that represents the finite extent of the annihilation region (radius 0.8 fm). The last two terms describe final state effects. P_{miss} is the probability that final state mesons do not interact or interact only elastically. This function excludes the annihilation events which produce highly excited A_t-2 or lighter final nuclei. Although calculations of P_{miss} are fairly involved, the net effect is close to a simple geometric estimate of an opening angle as seen by pions to avoid nuclear collisions [67]. Finally P_{dh} is a model correction for the rearrangement energy in the final nucleus. It excludes those captures that lead to A_t-1 nuclei excited above the particle emission or fission thresholds.

In the limit $P_{\mathrm{miss}}=1$, $P_{dh}=0$, and ρ_i equal to the total nuclear density Eq. (1) produces atomic level widths measured in the x-ray experiments. $\mathrm{Im}a_{N\bar{N}}$ is believed to represent an effective averaged antiproton-nucleon absorptive amplitude and is determined by a fit to atomic level widths and shifts. This number is not needed for studies of the neutron halo. What is needed is the ratio $R_{np}=\mathrm{Im}a_{n\bar{p}}/\mathrm{Im}a_{p\bar{p}}$ which, as indicated above, is taken as 0.63. (In Ref. [53] arguments to use the slightly different value $R_{np}=0.82$ were given. In the present paper we keep our previous [13] definition of the halo factor in order to facilitate the comparisons.) For the details of final state calculations and the derivation of the intuitively simple formula (1), we refer to Ref. [53]. One problem in the analysis of halo factors is to know the atomic state from which nuclear capture takes place. At this stage of research a complete answer is not available. One can calculate the distribution of these states for the lower part of the atomic cascade. This is possible for states $n<20$, i.e., states localized between the nucleus and electron cloud. In addition, this part of the cascade may be checked directly via measurements of x-ray intensities. It was concluded [53,68] that about 95% of the nuclear captures take place from levels with only one or two different values of the antiproton angular momentum l, although the distribution over n may involve more states. These l values correspond to circular orbits of the so-called ''upper'' and ''lower'' states of capture. (In hadronic atom terminology the ''lower-n'' state is the last state which can be observed before the strong interaction prevents further hadron cascading and x-ray emission. The ''upper'' level has the principal quantum number n, higher by 1 with respect to the ''lower'' level.) The difficulty is that these low-n captures come to at most half of the total

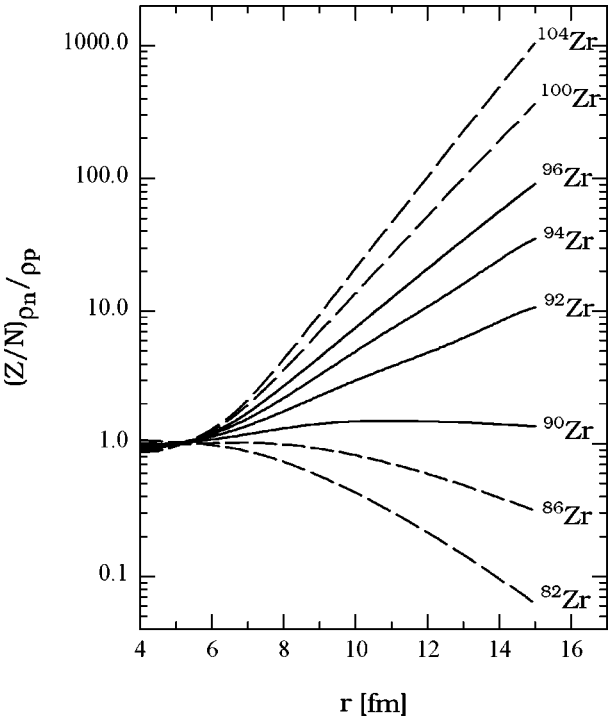

FIG. 9. The same as Fig. 7 for Zr isotopes. The dashed lines show the density ratio for the unstable Zr isotopes.

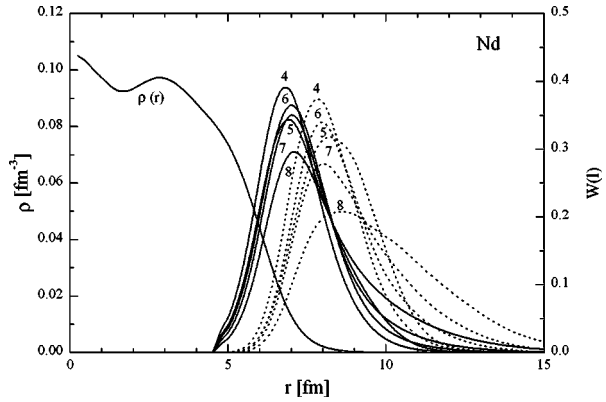

FIG. 10. Total probability densities (solid lines) for antiproton absorption from circular orbits in Nd as a function of the distance from the nuclear center, together with the corresponding cold-absorption densities (dashed lines). For these curves the scale labeled $W(l)$ holds. The numbers at the curves indicate the respective values of the orbital angular momentum. The total nuclear density $\rho(r)$ (left-hand scale) is also shown.

nuclear capture rate [69,70]. In our calculations the l distribution of capture states given by the low-n cascade calculations has been used.

The arguments in favor of this assumption are illustrated in Fig. 10. In this figure the calculated total absorption probability densities in antiprotonic Nd and the corresponding distributions for cold absorption (i.e., those leading to the production of A_t-1 nuclei) are shown for several states with different antiproton angular momentum. These densities are, for a given value of l, almost n independent. In the Nd atom the ''low-n'' capture takes place from the $l=6$ and $l=7$ states. The overlap of the antiproton wave function with the nucleus in these and higher-l states is localized at the nuclear surface by the centrifugal barrier. On the other hand, for lower values of l another localizing factor arises—the strong absorption of antiprotons. As a result, the radius of maximum absorption reaches some limiting value. This penetration blocking indicates that even if some of the antiprotons are absorbed from lower-l states, the spatial scenario of cold capture is not changed significantly.

C. Comparison of the experimental data with calculations

1. Annihilation site

As was indicated at the beginning of this paper, experiment determines the neutron to proton density ratio at the nuclear periphery, presumably at distances close to the antiproton annihilation site. The calculations mentioned above and presented in detail in Ref. [53] indicate that, almost independently of the target mass, the method is most sensitive for densities encountered at distances about 3 fm larger than the half-density radius. The width of the annihilation probability distribution [full width at half maximum (FWHM)] for events testing the density ratio is between 2 and 3 fm (compare also Fig. 10).

The experimental observable related to the annihilation site is the production yield of nuclei one mass unit lighter than the target mass. This yield, related to the annihilation geometry, depends strongly on the antiproton-nucleus interaction, pion-nucleus interaction, pion energy distribution, and kinematic correlations. Fortunately, it is rather insensitive to the neutron to proton density ratio, which affects mainly the second observable of this experiment.

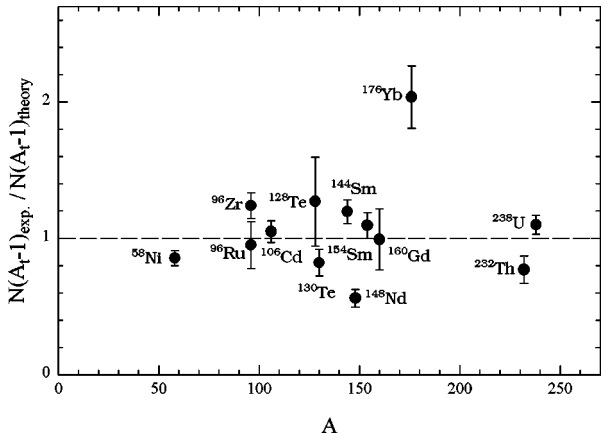

FIG. 11. Comparison of the experimentally determined yield of (A_t-1) nuclei with the calculated values.

The rather good agreement between the experimental data and theoretical estimate for the production yield of A_t-1 nuclei, presented in Fig. 11, indicates that all factors governing this production are to a large extent understood. However, the only large exception, the ^{176}Yb nucleus, for which the annihilation site seems to be located much farther away from the nucleus than predicted by calculations, needs further studies (cf. [53]).

2. Neutron to proton density ratio

Figure 12 shows a comparison between the experimentally determined and calculated values of the halo factor. Again, the agreement is fair although slightly less good than for the yield of A_t-1 products, indicating the need for some improvements in the nuclear density calculations. This is especially true for the two-''proton-halo'' nuclei ^{106}Cd and ^{144}Sm for which the HFB calculations predict a neutron-rich rather than a proton-rich atmosphere at large nuclear distances (see Fig. 7). On the contrary, the calculated neutron and proton densities in ^{176}Yb can be reasonably close to reality, the discrepancy between theory and experiment lying mainly in the underestimated annihilation distance.

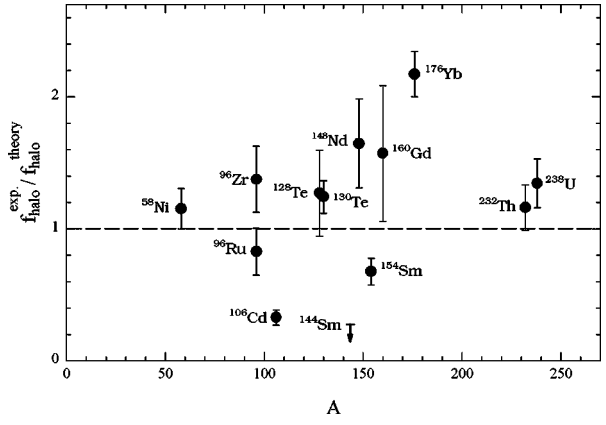

FIG. 12. Comparison of the experimentally determined halo factor with the calculated values.

3. Microscopic composition of the nuclear periphery from the isomeric ratio

Let us discuss, as an example, the case of the ^{129}Te isomeric ratio. We assume that the decay of the excited hole states in ^{129}Te after antiproton annihilation on the peripheral neutron proceeds without a parity change ($E1$ transitions much weaker than $M1$ and $E2$ ones). From calculations for the ^{130}Te target, as indicated above, one deduces that the annihilation site is located around $r=8.7$ fm in the case of the antiproton-neutron interaction. At this distance the ratio of the $1h11/2$ orbital density (main component of the high-spin isomer) to the sum of densities of the $2d3/2$ and other positive parity orbitals is 0.26. As no other negative parity orbitals contribute to the nuclear density at this distance this is the approximate theoretical expectation of the isomeric ratio, experimentally determined (cf. Table IV) to be 0.45 ± 0.15. In a more refined approach one would consider antiproton annihilation separately for each orbital (similarly, as was discussed in [56]) and calculate the sum of the corresponding negative and positive parity contributions. The assumption of the spectroscopic factors $S=1$ should not introduce any appreciable errors, as states belonging to the same orbital should be interconnected by fast gamma transitions.

Similar arguments applied to the ^{95}Tc isomeric ratio lead to a theoretical value equal to 0.28, to be compared with the experimental result of 0.58 ± 0.22.

VI. SUMMARY AND CONCLUSIONS

Using the recently proposed new method for the study of the nuclear periphery composition we have investigated a number of targets in the mass range from 58 to 238. The experimental data clearly indicate that the periphery of nuclei in which the neutron binding energy is smaller than about 10 MeV has more neutrons than would be expected from the target N/Z ratio. As almost all heavy stable isotopes of all elements exhibit a neutron binding energy smaller than the value quoted above, the neutron-rich periphery should be a quite common phenomenon for stable and even more for neutron-rich radioactive isotopes. However, the observation of this phenomenon may be difficult in experiments in which the nuclear periphery is tested with methods less sensitive than offered by strongly interacting probes. Indeed, calculations based on the antiproton-nucleus and pion-nucleus interactions indicate that the method used in the present work is sensitive at nuclear distances around 3 fm larger than the nuclear half-density radius. At these distances the nuclear density is about 100–1000 times smaller than the central one, which leads to evident experimental difficulties.

In the two cases investigated in this work it was found that the outer periphery of the nuclei studied (^{106}Cd and ^{144}Sm) exhibits a proton-rich atmosphere. Although this result may be understood intuitively at least for the closed neutron shell nucleus ^{144}Sm, it contradicts the nuclear periphery composition expected from the Hartree-Fock-Bogoliubov calculation performed in this work. Therefore it can probably be used as a sensitive test for the nuclear periphery models.

The experimentally determined isomeric ratio for nuclei one mass unit lighter than the target mass will probably constitute a similarly sensitive test for modeling the nuclear periphery. If this happens to be true, a number of other cases could be investigated in the near future using the new antiproton facility at CERN.

ACKNOWLEDGMENTS

Our thanks are due to Peter Maier-Komor, Anna Stolarz, and Katharina Nacke for their invaluable help in preparing the targets and to Anna Grochulska, who participated at the early stage of this work. We also gratefully acknowledge fruitful discussions with Jacek Dobaczewski and Janusz Skalski. The competent and efficient help of the LEAR staff during the irradiations was crucial for the success of this work. The present paper summarizes the results of many years of experiments and evaluations which were continuously supported by research and travel grants from the Polish State Committee for the Scientific Research, by the Joint Project of Science and Technology Cooperation between Germany and Poland, and recently by a grant from the Volkswagen Foundation.

[1] D. H. Wilkinson, Philos. Mag. **4**, 215 (1959).
[2] D. H. Davis, S. P. Lovell, M. Csejthey-Barth, J. Sacton, G. Schorochoff, and M. O'Reilly, Nucl. Phys. **B1**, 434 (1967).
[3] E. H. S. Burhop, Nucl. Phys. **B1**, 438 (1967).
[4] E. H. S. Burhop, D. H. Davis, J. Sacton, and G. Schorochoff, Nucl. Phys. **A132**, 625 (1969).
[5] J. A. Nolen, Jr. and J. P. Schiffer, Annu. Rev. Nucl. Sci. **19**, 471 (1969).
[6] H. J. Körner and J. P. Schiffer, Phys. Rev. Lett. **27**, 1457 (1971).
[7] E. H. S. Burhop, Nucl. Phys. **B44**, 445 (1972).
[8] W. M. Bugg, G. T. Condo, E. L. Hart, H. O. Cohn, and R. D. McCulloch, Nucl. Phys. **B64**, 29 (1973).
[9] W. M. Bugg, G. T. Condo, E. L. Hart, H. O. Cohn, and R. D. McCulloch, Phys. Rev. Lett. **31**, 475 (1973).
[10] M. Leon and R. Seki, Phys. Lett. **48B**, 173 (1974).
[11] W. M. Bugg, G. T. Condo, E. L. Hart, and H. O. Cohn, Phys. Rev. Lett. **35**, 611 (1975).
[12] J. Jastrzębski, H. Daniel, T. von Egidy, A. Grabowska, Y. S. Kim, W. Kurcewicz, P. Lubiński, G. Riepe, W. Schmid, A. Stolarz, and S. Wycech, Nucl. Phys. **A558**, 405c (1993).
[13] P. Lubiński, J. Jastrzębski, A. Grochulska, A. Stolarz, A. Trzcińska, W. Kurcewicz, F. J. Hartmann, W. Schmid, T. von Egidy, J. Skalski, R. Smolańczuk, S. Wycech, D. Hilscher, D. Polster, and H. Rossner, Phys. Rev. Lett. **73**, 3199 (1994).
[14] J. P. Adams, B. Castel, and H. Sagawa, Phys. Rev. C **53**, 1016 (1996).
[15] H. A. Bethe and P. J. Siemens, Nucl. Phys. **B21**, 589 (1970).
[16] J. W. Negele, Phys. Rev. C **1**, 1260 (1970).
[17] A. Bohr and B. R. Mottelson, *Nuclear Structure* (Benjamin,

New York, 1969), Vol. 1, Chap. 2.
[18] D. F. Jackson, J. Phys. (Paris), Colloq. **36**, C5-1 (1975).
[19] I. Angeli and R. J. Lombard, Z. Phys. A **324**, 299 (1986).
[20] Y. K. Gambhir, P. Ring, and A. Thimet, Ann. Phys. (N.Y.) **198**, 132 (1990).
[21] A. Baran, J. L. Egido, B. Nerlo-Pomorska, K. Pomorski, P. Ring, and L. M. Robledo, J. Phys. G **21**, 657 (1995).
[22] C. J. Batty, E. Friedman, H. J. Gils, and H. Rebel, Adv. Nucl. Phys. **19**, 1 (1989).
[23] A. Krasznahorkay, J. Bacelar, J. A. Bordewijk, S. Brandenburg, A. Buda, G. van't Hof, M. A. Hofstee, S. Kato, T. D. Poelhekken, S. Y. van der Werf, A. van der Woude, M. N. Harakeh, and N. Kalantar-Nayestanaki, Phys. Rev. Lett. **66**, 1287 (1991).
[24] J. Dobaczewski, W. Nazarewicz, and T. R. Werner, Z. Phys. A **354**, 27 (1996).
[25] J. Dobaczewski, W. Nazarewicz, T. R. Werner, J. F. Berger, C. R. Chinn, and J. Dechargé, Phys. Rev. C **53**, 2809 (1996).
[26] I. Hamamoto, H. Sagawa, and X. Z. Zhang, Phys. Rev. C **53**, 765 (1996).
[27] J. Takahashi, M. Munhoz, E. M. Szanto, N. Carlin, N. Added, A. A. P. Suaide, M. M. de Moura, R. Liguori Neto, A. Szanto de Toledo, and L. F. Canto, Phys. Rev. Lett. **78**, 30 (1997).
[28] G. Backenstoss, J. Egger, H. Koch, H. P. Povel, A. Schwitter, and L. Tauscher, Nucl. Phys. **B73**, 189 (1974).
[29] Th. Köhler, P. Blüm, G. Büche, A. D. Hancock, H. Koch, A. Kreissl, H. Poth, U. Raich, D. Rohmann, G. Backenstoss, Ch. Findeisen, J. Repond, L. Tauscher, A. Nilson, S. Carius, M. Suffert, S. Charalambus, M. Chardalas, S. Dedoussis, H. Daniel, T. von Egidy, F. J. Hartmann, W. Kanert, G. Schmidt, J. J. Reidy, M. Nicholas, and A. Wolf, Phys. Lett. B **176**, 327 (1986).
[30] C. Garcia-Recio, J. Nieves, and E. Oset, Nucl. Phys. **A547**, 473 (1992).
[31] C. J. Batty, E. Friedman, and A. Gal, Nucl. Phys. **A592**, 487 (1995).
[32] U. Gastaldi, K. Kilian, and G. Plass, Report No. CERN/PSCC/79-17, 1979.
[33] P. Lefèvre, in *Physics at LEAR with Low-Energy Antiprotons*, Proceedings of the 4th LEAR Workshop, Villars-sur-Ollon, edited by C. Amsler *et al.* (Harwood Academic, Chur, Switzerland, 1987), p. 19.
[34] E. Jones, in *Physics at LEAR with Low-Energy Antiprotons* [33], p. 7.
[35] E. F. Moser, H. Daniel, T. von Egidy, F. J. Hartmann, W. Kanert, G. Schmidt, M. Nicholas, and J. J. Reidy, Phys. Lett. B **179**, 25 (1986).
[36] E. F. Moser, H. Daniel, T. von Egidy, F. J. Hartmann, W. Kanert, G. Schmidt, Ye. S. Golubeva, A. S. Iljinov, M. Nicholas, and J. J. Reidy, Z. Phys. A **333**, 89 (1989).
[37] T. von Egidy, H. Daniel, F. J. Hartmann, W. Kanert, E. F. Moser, Ye. S. Golubeva, A. S. Iljinov, and J. J. Reidy, Z. Phys. A **335**, 451 (1990).
[38] J. Jastrzębski, W. Kurcewicz, P. Lubiński, A. Grabowska, A. Stolarz, H. Daniel, T. von Egidy, F. J. Hartmann, P. Hofmann, Y. S. Kim, A. S. Botvina, Ye. S. Golubeva, A. S. Iljinov, G. Riepe, and H. S. Plendl, Phys. Rev. C **47**, 216 (1993).
[39] J. Jastrzębski, P. Lubiński, and A. Trzcińska, Acta Phys. Pol. B **26**, 527 (1995).
[40] P. Lubiński *et al.* (unpublished).
[41] J. B. Cumming, P. E. Haustein, R. W. Stoenner, L. Mausner, and R. A. Naumann, Phys. Rev. C **10**, 739 (1974).
[42] L. Pieńkowski, J. Jastrzębski, W. Kurcewicz, A. Gizon, J. Blachot, and J. Crançon, Phys. Rev. C **43**, 1331 (1991).
[43] P. E. Haustein and T. J. Ruth, Phys. Rev. C **18**, 2241 (1978).
[44] Y. Eisenberg and D. Kessler, Nuovo Cimento **19**, 1195 (1961).
[45] M. Leon and R. Seki, Nucl. Phys. **A282**, 445 (1977).
[46] M. Leon and R. Seki, Nucl. Phys. **A282**, 461 (1977).
[47] M. R. Clover, R. M. DeVries, N. J. DiGiacomo, and Y. Yariv, Phys. Rev. C **26**, 2138 (1982).
[48] A. S. Iljinov, V. I. Nazaruk, and S. E. Chigrinov, Nucl. Phys. **A382**, 378 (1982).
[49] J. Cugnon and J. Vandermeulen, Nucl. Phys. **A445**, 717 (1985).
[50] J. Cugnon, P. Deneye, and J. Vandermeulen, Nucl. Phys. **A500**, 701 (1989).
[51] D. Polster, D. Hilscher, H. Rossner, T. von Egidy, F. J. Hartmann, J. Hoffmann, W. Schmid, I. A. Pshenichnov, A. S. Iljinov, Ye. S. Golubeva, H. Machner, H. S. Plendl, A. Grochulska, J. Jastrzębski, W. Kurcewicz, P. Lubiński, J. Eades, and S. Neumaier, Phys. Rev. C **51**, 1167 (1995).
[52] J. Cugnon, P. Jasselette, and J. Vandermeulen, Nucl. Phys. **A470**, 558 (1987).
[53] S. Wycech, J. Skalski, R. Smolańczuk, J. Dobaczewski, and J. R. Rook, Phys. Rev. C **54**, 1832 (1996).
[54] P. E. Hodgson, Contemp. Phys. **22**, 511 (1981).
[55] J. Błocki and W. Świątecki (private communication).
[56] S. D. Bloom, M. S. Weiss, and C. M. Shakin, Phys. Rev. C **5**, 238 (1972).
[57] E. Browne and R. B. Firestone, in *Table of Radioactive Isotopes*, edited by V.S. Shirley (Wiley, New York, 1986).
[58] P. Lubiński, Ph.D. thesis, Warsaw University, 1997 (unpublished).
[59] P. Lubiński, Heavy Ion Laboratory Report No. 2/97, Warsaw University, 1997.
[60] M. Wade and V. G. Lind, Phys. Rev. D **14**, 1182 (1976).
[61] R. G. Helmer, Nucl. Data Sheets **72**, 83 (1994).
[62] F. Balestra, S. Bossolasco, M. P. Bussa, L. Busso, L. Ferrero, D. Panzieri, G. Piragino, F. Tosello, R. Barbieri, G. Bendiscioli, A. Rotondi, P. Salvini, A. Zenoni, Yu. A. Batusov, I. V. Falomkin, G. B. Pontecorvo, M. G. Sapozhnikov, V. I. Tretyak, C. Guaraldo, A. Maggiora, E. Lodi Rizzini, A. Haatuft, A. Halsteinslid, K. Myklebost, J. M. Olsen, F.O. Breivik, T. Jacobsen, and S. O. Sorensen, Nucl. Phys. **A491**, 572 (1989).
[63] W. J. Gerace, M. M. Sternheim, and J. F. Walker, Phys. Rev. Lett. **33**, 508 (1974).
[64] A. Baran, K. Pomorski, and M. Warda, Z. Phys. A **357**, 33 (1997).
[65] J. Dobaczewski, H. Flocard, and J. Treiner, Nucl. Phys. **A422**, 103 (1984).
[66] C. A. Stone and W. B. Walters, Z. Phys. A **328**, 257 (1987).
[67] J. Cugnon (private communication).
[68] S. Wycech and R. Smolańczuk, Few-Body Syst., Suppl. **99**, 1 (1995).
[69] C. E. Wiegand and G. L. Godfrey, Phys. Rev. A **9**, 2282 (1974).
[70] A. Trzcińska *et al.* (unpublished).
[71] J. F. Janni, At. Data Nucl. Data Tables **27**, 147 (1982).